

Diffusion-vortex composite phase metasurface for broadband RCS reduction

Original

Diffusion-vortex composite phase metasurface for broadband RCS reduction / Li, Z., Wang, J., Li, Y.. - In: OPTICAL MATERIALS EXPRESS. - ISSN 2159-3930. - 16:4(2026), pp. 1015-1028. [10.1364/ome.589263]

Availability:

This version is available at: 11583/3012628 since: 2026-07-02T12:12:18Z

Publisher:

Optica Publishing Group

Published

DOI:10.1364/ome.589263

Terms of use:

This article is made available under terms and conditions as specified in the corresponding bibliographic description in the repository

Publisher copyright

(Article begins on next page)



Diffusion-vortex composite phase metasurface for broadband RCS reduction

ZHAOHUA LI, JUNHONG WANG,* AND YUJIAN LI

The Key Laboratory of All Optical Network and Advanced Telecommunication Network, Ministry of Education, Institute of Lightwave Technology, Beijing Jiaotong University, Beijing 100044, China
*wangjunh@bjtu.edu.cn

Abstract: This paper proposes a composite phase approach that combines the diffusion phase and vortex phase to design a broadband metasurface for reducing the radar cross section (RCS) of circularly polarized waves. The gradient phase distributions of metasurface unit cells for converting circularly polarized incident waves into co-polarized reflected waves are realized by the Pancharatnam-Berry (PB) phase method. The diffusion phase distribution is employed to achieve uniform scattering within a specified solid-angle region, while the superimposed vortex phase is introduced to generate a reflection null in the normal direction of the metasurface. These dual-phase mechanisms synergistically deflect the scattered energy away from monostatic radar reception angles, thereby significantly reducing backward RCS and enhancing stealth capability against circularly polarized wave detection. Simulation results demonstrate that under normal incidence of left-handed circularly polarized (LCP) waves, the metasurface achieves an RCS reduction exceeding 10 dB for right-handed circularly polarized (RCP) waves over the frequency range from 12.63 GHz to 18.1 GHz, while the RCS of the LCP component remains at an extremely low level. Furthermore, conformal application of the metasurface on cylindrical surfaces preserves the central null characteristic in co-polarized diffuse scattering. The proposed composite phase methodology provides a novel way for wide-angle and multidimensional stealth technologies in complex electromagnetic environments.

© 2026 Optica Publishing Group under the terms of the [Optica Open Access Publishing Agreement](#)

1. Introduction

The rapid advancement of electromagnetic wave manipulation technology has enabled transformative progress in target scattering control, stealth technology, and radar cross-section (RCS) reduction. Minimizing the RCS through electromagnetic absorption, beam redirection, or tailored specific scattering suppression has become a critical challenge in applied electromagnetics, thereby stimulating extensive research into advanced stealth mechanisms [1–3]. Conventional stealth approaches based on geometric shaping or absorbing coatings suffer from inherent limitations in practical applications [4]. Benefiting from their unique electromagnetic properties, metasurfaces offer a promising and flexible platform for RCS control and have consequently emerged as a major research focus [5,6]. Existing metasurface-based RCS reduction strategies mainly include electromagnetic absorption [7,8], polarization conversion [9,10], phase cancellation [11,12], and coding metasurfaces [13,14]. Previous studies have primarily focused on suppressing the co-polarized components of linear polarized waves, while investigations into the scattering characteristics of circularly polarized (CP) waves remain relatively scarce.

To address the specific requirements for CP wave scattering suppression, the Pancharatnam-Berry (PB) phase demonstrates distinctive advantages. The PB phase refers to an additional phase shift arising from accumulation of the polarization state evolves along the propagation path when CP waves propagate through anisotropic media [15–17]. This mechanism enables efficient manipulation of CP waves through simple rotational control of anisotropic unit patterns. By spatially distributing PB phase gradients, precise electromagnetic wavefront control can be achieved, thereby realizing functionalities such as beam deflection [18] and focusing [19]. When a

target is illuminated by circularly polarized electromagnetic waves, polarization conversion effect occurs, resulting in reflected waves with cross-polarized components. However, conventional metasurface-based RCS reduction strategies typically rely on converting incident CP waves into co-polarized reflections to suppress cross-polarized scattering. Such polarization conversion, nevertheless, inevitably leads to enhanced co-polarized reflected energy, thereby increasing detectability by monostatic radar systems [20,21]. Therefore, the simultaneous suppression of both cross-polarized and converted co-polarized scattering components becomes a critical challenge.

The unique scattering characteristics of vortex beams carrying orbital angular momentum (OAM) present new possibilities to overcome these limitations [22,23]. Although OAM beams have been extensively investigated for capacity enhancement in near-field communication systems owing to their mode orthogonality [24], their application in RCS reduction has recently emerged as a significant research hotspot in electromagnetic stealth. Cutting-edge metasurface designs have demonstrated effective broadband scattering suppression by leveraging vortex singularities and OAM-based composite phase modulation [25–27]. Vortex beams exhibit an annular energy distribution with nearly zero field intensity at the beam center as a result of the inherent phase singularity [28]. Various techniques have been developed for vortex beam generation, including spiral phase plates [29], antenna arrays [30], and metasurfaces [31,32]. Considering that PB phase-gradient metasurfaces offer distinctive advantages such as ultrathin profiles, low fabrication complexity, and ease of integration compared with conventional approaches, the combination of gradient phase scattering and vortex beam generation is expected to provide an effective route for suppressing backward scattering of both co-polarized and cross-polarized CP waves. Furthermore, in practical aerospace applications, modern stealth targets rarely consist of purely planar surfaces. Instead, they feature complex, curved aerodynamic profiles designed for optimal flight performance. Developing conformal metasurfaces capable of maintaining robust RCS reduction performance when wrapped around curved structures has become a critical requirement for advanced stealth technologies.

This paper proposes a coordinated scattering control methodology that combines gradient diffusion phase and vortex phase. A double-helix unit cell is designed, and the phase arrangement of the metasurface is realized through the joint implementation of diffusion and vortex phase distributions. The diffusion phase enables uniform energy scattering within predetermined angular regions, whereas the vortex phase generates a conical scattering beam featuring a central null. This dual-phase strategy overcomes the limitations of conventional methods that suppress only either co-polarized or cross-polarized scattering of CP waves. Under CP wave illumination, the proposed metasurface achieves broadband cross-polarized RCS reduction while maintaining an ultralow co-polarized RCS in backward directions, thereby providing an effective solution against full-polarization detection threats in complex electromagnetic environments.

2. Composite phase principle and metasurface simulation analysis

2.1. Principle of diffusion-vortex composite phase

The PB phase is an important mechanism for wavefront control of CP waves. For unit patches exhibiting 180° rotational symmetry, when a CP wave is incident, the reflection coefficients of

the reflected waves can be derived from the reflection Jones matrix and are expressed as [33]:

$$\begin{aligned}
 r_{ll}(\alpha) &= \frac{1}{2}[(r_{xx} - r_{yy}) + j(r_{xx} + r_{yy})]e^{-2j\alpha} \\
 r_{rl}(\alpha) &= \frac{1}{2}[(r_{xx} + r_{yy}) - j(r_{xx} - r_{yy})] \\
 r_{lr}(\alpha) &= \frac{1}{2}[(r_{xx} + r_{yy}) + j(r_{xx} - r_{yy})] \\
 r_{rr}(\alpha) &= \frac{1}{2}[(r_{xx} - r_{yy}) - j(r_{xx} + r_{yy})]e^{2j\alpha}
 \end{aligned} \tag{1}$$

where r_{ll}/r_{rl} and r_{rr}/r_{lr} denote the co-polarized and cross-polarized reflection coefficients corresponding to left-handed circularly polarized (LCP) and right-handed circularly polarized (RCP) incident waves, respectively, while r_{xx}/r_{yx} and r_{xy}/r_{yy} represent the reflection coefficients for x - and y -polarized incident waves. When the resonator patch in the metasurface unit is rotated by an angle α , Eq. (1) indicates that the co-polarized reflection coefficient acquires an additional phase term $e^{\pm 2j\alpha}$, resulting in phase shifts of -2α and $+2\alpha$ for the reflected LCP and RCP waves, respectively. Consequently, by rotating the resonator patches with different angle α , the desired phase distribution of the metasurface can be precisely engineered based on the PB phase principle.

To achieve RCS reduction, diffuse scattering of incident electromagnetic waves is commonly realized by arranging the phases of metasurface unit cells according to a diffusion phase distribution. This distribution introduces position-dependent variations in the energy propagation direction and transforms the reflected wavefront from a planar profile into a quasi-spherical one. Consequently, the incident plane wave is redirected into free space with nearly uniform diffusion, effectively decoupling the reflected energy from the specular direction and redistributing it uniformly within a predefined solid-angle region. The diffuse phase φ_{diffuse} is expressed as:

$$\varphi_{\text{diffuse}} = \frac{k_0(x^2 + y^2)}{\gamma} \tag{2}$$

where k_0 denotes the free-space wave number, and (x, y) represent the two-dimensional planar coordinates of the metasurface unit cell. For the purpose of phase synthesis, these coordinates are normalized with respect to the metasurface aperture size. The parameter γ is defined as a dimensionless diffusion coefficient that controls the spatial phase gradient and therefore the angular redistribution strength of the scattered field. Under this definition, the phase term φ_{diffuse} is dimensionless. The diffuse phase introduces a radially symmetric phase gradient that reshapes the shape of the reflected wave front, thereby governing the beam divergence characteristics. Owing to this curved wavefront, the reflected beam gradually spreads during propagation. Figure 1 schematically illustrates the diffusion behavior of electromagnetic waves modulated by φ_{diffuse} . The degree of beam diffusion can be flexibly controlled by adjusting the value of γ .

To physically elucidate the decoupling mechanism of the diffusion phase, we refer to the Generalized Snell's Law [34]. The quadratic phase profile defined in Eq. (2) acts mathematically equivalent to a virtual convex mirror. For a normally incident wave, the local reflection angle θ at any radial position is governed by the local phase gradient:

$$\sin(\theta) = \frac{1}{k_0} \frac{d\varphi_{\text{diffuse}}}{dr} = \frac{2r}{\gamma} \tag{3}$$

where $r = \sqrt{x^2 + y^2}$ denotes the radial coordinate in the same normalized aperture coordinate system. Unlike a flat perfect electric conductor (PEC) plate, the proposed phase profile provides

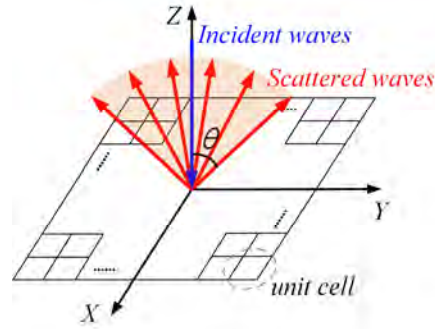


Fig. 1. Schematic diagram of diffusion waves modulation by the diffusion phase φ_{diffuse} .

a continuously varying gradient proportional to the radius r . This mechanism continuously redirects the incident electromagnetic energy into a broad range of reflection angles. Furthermore, the maximum diffusion angle θ_{max} occurs at the edge of the metasurface aperture r_{max} and can be quantitatively expressed as:

$$\theta_{\text{max}} = \arcsin\left(\frac{2r_{\text{max}}}{\gamma}\right) \quad (4)$$

Here r_{max} represents the maximum radial coordinate within the metasurface aperture in the same normalized coordinate system. For the metasurface considered in this work, the selected parameter range $\gamma=1, 5, \text{ and } 10$ ensures that the condition $2r_{\text{max}}/\gamma \leq 1$ is satisfied. This demonstrates that the beam diffusion angle is inversely proportional to the coefficient γ . Therefore, a smaller γ yields a steeper phase gradient and broader angular diffusion, whereas a larger γ confines the scattered energy to a narrower angular region.

The vortex phase is realized by arrangement metasurface unit cells with prescribed rotation angles α . The corresponding vortex phase distribution for OAM wave generation can be calculated as follow:

$$\varphi_{\text{vortex}} = l \arctan\left(\frac{y}{x}\right) \quad (5)$$

where l denotes the order of vortex wave. According to the principle of phase superposition, the total phase obtained by combining the diffusion wave and the vortex wave can be expressed as:

$$\varphi_{\text{total}} = \varphi_{\text{diffuse}} + \varphi_{\text{vortex}} \quad (6)$$

By arranging the metasurface unit cells with different rotation orientations according to the composite phase distribution matrix defined in the above equations, simultaneous reflection diffusion and vortex modulation of circularly polarized waves can be achieved. When the diffusion phase is superimposed with the vortex phase, the metasurface exhibits a dual mechanism of energy dilution and polarization interference.

2.2. Design of metasurface unit cell

A metal-dielectric-metal sandwiched metasurface structure is proposed, and the corresponding unit cell configuration is illustrated in Fig. 2. The top layer consists of a patch resonator formed by double-helical strips. The middle dielectric layer is composed of F4B with a relative permittivity of 2.65 and a loss tangent of 0.002. The bottom layer is a continuous metallic ground plane. Both the patch and the ground plane are made of copper with a thickness of 0.036 mm and a conductivity of $\sigma = 5.96 \times 10^7$ S/m. The optimized parameters of the unit cell are $p = 11$ mm, $h = 2.5$ mm, $g = 0.5$ mm, $w = 1.1$ mm, $l_1 = 1.85$ mm, $l_2 = 3.9$ mm and $l_3 = 4.4$ mm. The helix strip width $w = 1.1$ mm and patch gap $g = 0.5$ mm are uniform across the unit.

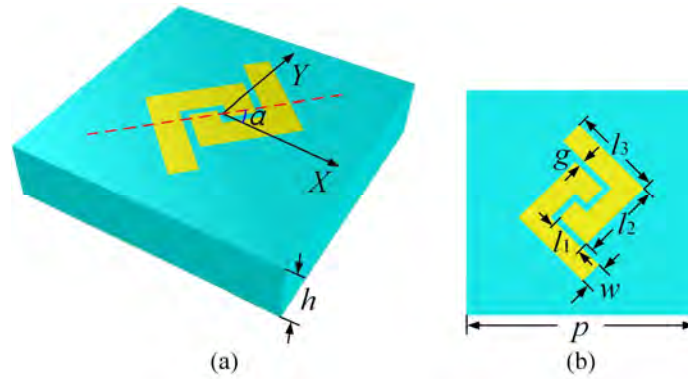


Fig. 2. Diagram of metasurface unit cell, (a) 3D structure, and (b) top view.

The metasurface unit cell is modeled and simulated with periodic boundary conditions applied along both x - and y -axis directions. Under normal incidence of CP waves, the simulated amplitude and phase responses of co-polarized and cross-polarized reflection coefficients are shown in Fig. 3. As shown in Fig. 3(a), when illuminated by LCP waves, the normalized magnitude of the co-polarized reflection coefficient remains exceeds 0.8 over the frequency range from 12.3 GHz to 20.19 GHz, indicating efficient LCP-to-LCP reflection. According to PB phase theory, the rotational angle α of resonators introduces an additional phase term $e^{-2j\alpha}$ to the co-polarized reflected wave. As illustrated in Fig. 3(b), a rotational increment of 15° in α results in a corresponding phase difference of 30° between the co-polarized reflection coefficients r_{ll} of adjacent unit cells. Consequently, by employing 12 distinct phase-gradient unit cells, a complete phase coverage of 2π can be achieved. Based on this property, the metasurface phase distribution can be precisely engineered using the calculated diffusion and vortex phase profiles to realize the desired wavefront manipulation.

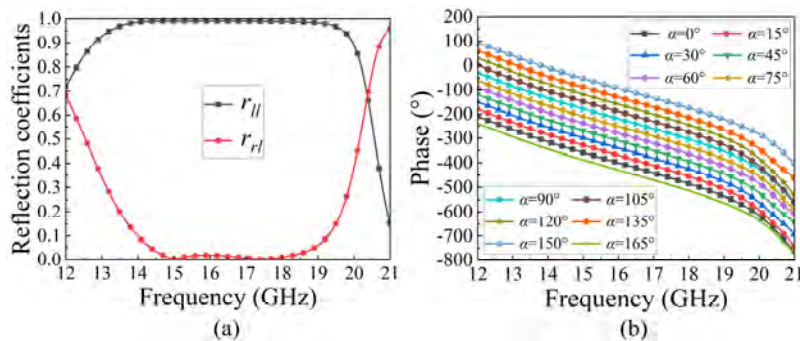


Fig. 3. Reflection coefficients of unit cell under LCP wave incidence, (a) normalized amplitude, and (b) phase of the co-polarized reflection coefficients.

2.3. Simulation of composite phase metasurface

The performance of the metasurface employing the diffusion phase is analyzed first. Based on the diffusion phase φ_{diffuse} defined in Eq. (2), the corresponding gradient phase distribution matrix of the metasurface is calculated, and a 30×30 array composed of resonator unit cells with a 15° rotational phase gradient is designed. This configuration enables effective wavefront

manipulation under normal incidence of CP waves. Figure 4 presents the 3D far-field scattering patterns of the diffusion-phase metasurfaces with different diffusion coefficients. The results show that the diffusion-phase metasurface redistributes the incident CP waves uniformly toward the upper half-space. As the diffusion coefficient γ increases from 1 to 10, the diffusion region gradually evolves from near-omnidirectional scattering to confinement within specific solid-angle regions, while preserving a nearly uniform energy distribution within the designated angular ranges. By adjusting the diffusion coefficient, the beam divergence can be precisely controlled, enabling uniform scattering of incident CP waves over predefined angular regions.

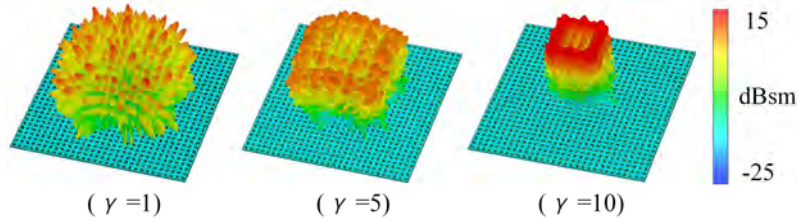


Fig. 4. 3D far-field images of diffusion-phase metasurface with different diffusion-coefficients.

To further suppress the specular reflection peak along the metasurface normal direction, vortex phase modulation is introduced to redistribute the reflected energy into annular scattering lobes. This redistribution effectively steers the scattered energy away from monostatic radar reception angles and leads to a pronounced reduction in backward RCS. Following the principle of phase superposition in Eq. (6), a composite phase profile is generated by combining the diffusion phase and the vortex phase, thereby forming the diffusion-vortex metasurface. Figure 5 depicts the resulting composite phase distribution obtained by superimposing a diffusion phase with $\gamma=1$ and a vortex phase with topological charge $l=2$. The metasurface is constructed by arranging gradient-phase units according to the calculated composite phase distribution. Under normal incidence of LCP waves, 3D far-field scattering patterns of the composite-phase metasurface at 13.4 GHz are obtained for different combinations of γ and l , as shown in Fig. 6. As the vortex order increases from $l=2$ to $l=4$, the phase singularity effect becomes more pronounced, resulting in enlarged beam divergence angles and expanded central null regions. Meanwhile, increasing the diffusion coefficient γ from 1 to 10 causes the reflected scattering pattern to transition from nearly omnidirectional diffusion to confinement within specific angular sectors. Due to the inherent central null effect of the vortex phase, the scattered field exhibits an annular profile resembling that of a vortex beam. This dual-phase modulation strategy enables dynamic control of beam null radii and lobe density through coordinated adjustment the parameters l and γ . In this dual-phase modulation scheme, the diffusion phase governs the overall angular spread of the scattered energy, whereas the vortex phase suppresses specular backscattering, jointly redirecting the reflected energy away from monostatic radar detection zones and enabling substantial RCS reduction.

Figure 7 presents the monostatic RCS as a function of frequency for both LCP and RCP reflected waves from composite-phase metasurfaces with different diffusion coefficients under normal incidence of LCP wave. When LCP wave is normally incident on a PEC surface, the reflected wave is converted into the RCP (cross-polarized) state. However, the proposed metasurface functions as a polarization converter, transforming the incident LCP wave primarily into a reflected LCP (co-polarized) wave. Consequently, the cross-polarized component is inherently reduced relative to the PEC baseline due to this polarization conversion. The critical challenge for RCS reduction then becomes the suppression of the converted co-polarized energy. As shown in Fig. 7(a), compared with a PEC plate of the same size, the proposed diffusion-vortex composite-phase

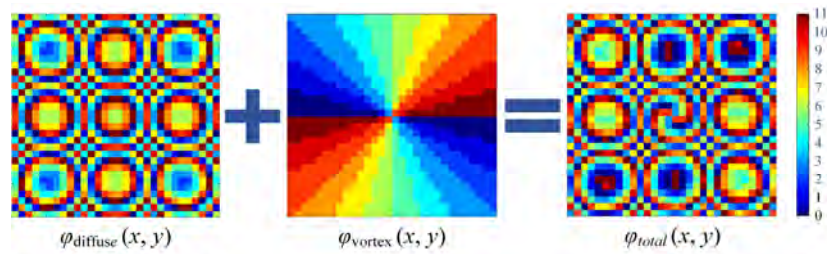


Fig. 5. Composite phase distribution superimposed by the diffusive phase and vortex phase.

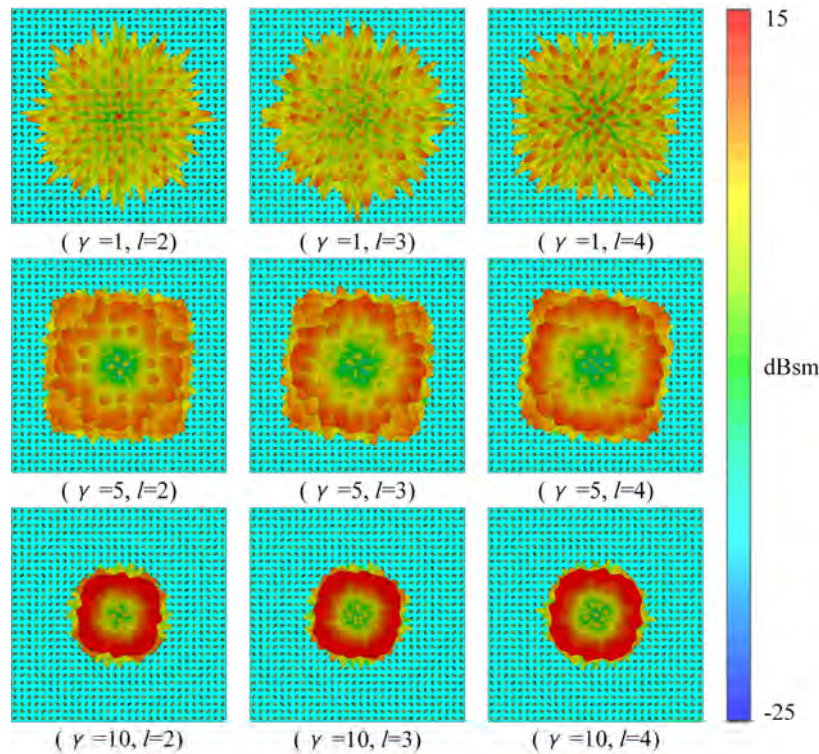


Fig. 6. 3D scattering far-field patterns of the diffusion-vortex metasurface for different combinations of the diffusion coefficient γ and vortex order l at 13.4 GHz.

metasurface achieves more than 10 dB RCS reduction in backscattered RCP component over the frequency range from 12.4 GHz to 17.3 GHz under LCP illumination. With an increasing diffusion coefficient γ , the vortex phase plays a significant role in redistributing reflected energy into annular scattering beams, resulting in enhanced monostatic RCS suppression of up to 20 dB along the normal direction. Departing from traditional CP-conversion metasurfaces that concentrate on cross-polarization control, our strategy leverages the high polarization conversion ratio of the unit structure to maintain low RCP levels, while simultaneously employing a diffusion-vortex phase distribution to suppress LCP scattering, thereby achieving superior overall RCS reduction. The metasurface maintains uniformly distributed co-polarized scattering within the designated angular sectors while keeping the backward reflection level consistently below that of the PEC reference, as shown in Fig. 7(b). This simultaneous reduction of co-polarized and cross-polarized

scattering components demonstrates the effectiveness of the proposed approach for broadband stealth applications. The proposed diffusion-vortex phase strategy effectively redistributes this co-polarized energy into the spatial background, thereby achieving a low RCS level for both polarization components.

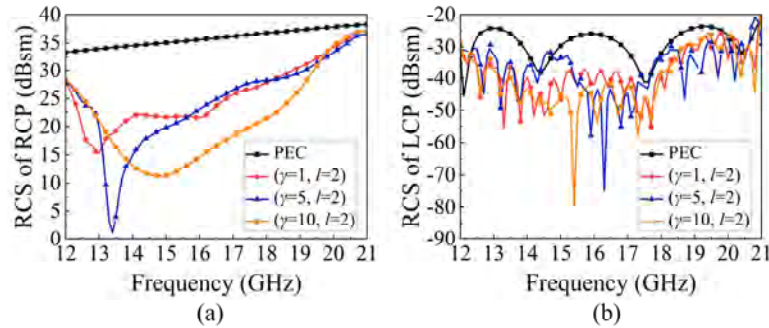


Fig. 7. Monostatic RCS of the metasurface with different diffusion-vortex coefficients for LCP wave incident. (a) RCP, (b) LCP.

To highlight the necessity of the proposed dual-phase modulation, a comparative analysis is conducted among pure diffusion, pure vortex, and composite metasurfaces. As shown in Fig. 8(a), in the exact normal direction, the pure vortex metasurface ($l=2$) indeed exhibits a deeper monostatic RCS reduction than both the pure diffusion and the composite metasurfaces. This occurs because the pure vortex phase possesses perfect mode purity, creating an absolute electromagnetic null at center. In contrast, the introduction of the diffusion phase inevitably degrades the OAM mode purity and introduces an $l=0$ component. However, for practical stealth applications, evaluating only the monostatic RCS is insufficient. While the composite phase sacrifices the unnecessarily deep monostatic null of the pure vortex design, it still maintains a highly effective monostatic reduction of over 20 dB. As illustrated in Fig. 8(b), the energy reflected by the pure vortex metasurface forms a tightly concentrated high-intensity ring-shaped beam in the bistatic scattering patterns at 13.4 GHz. While a pure vortex metasurface theoretically exhibits an ultra-deep monostatic null at the normal direction, it inevitably reflects energy into a high-intensity ring-shaped beam, significantly increasing the bistatic RCS and vulnerability to multistatic radar detection. The proposed diffusion-vortex strategy alleviates this limitation by breaking the concentrated ring-shaped scattering of the pure vortex phase into a broader and more distributed angular pattern. The composite phase is not intended to produce lower bistatic scattering than the pure vortex phase at every observation angle. Instead, its function is to mitigate the concentrated high-intensity annular scattering of the pure vortex case and redistribute the reflected energy more uniformly. By introducing the diffusion phase, the concentrated ring-shaped side lobes are effectively broken down and scattered into a wide angular domain. Simultaneously, the vortex phase maintains a superior normal monostatic reduction compared to a pure diffusion surface. This coordinated control provides a more balanced trade-off between monostatic suppression and bistatic scattering redistribution, especially in the near-normal angular region.

In practical applications, stealth targets with complex geometries often incorporate cylindrical structures. It is therefore important to investigate the electromagnetic scattering behavior of diffusion-vortex composite-phase metasurfaces under cylindrical conformal configurations. Figure 9 presents the far-field scattering characteristics at 15 GHz for three parameter combinations ($\gamma=1, l=2$), ($\gamma=5, l=2$) and ($\gamma=10, l=2$), which the metasurfaces are conformed to a cylindrical surface with a radius of curvature of 300 mm. The simulation results demonstrate that under normal incidence of LCP wave, the conformal metasurfaces effectively diffuse the reflected LCP

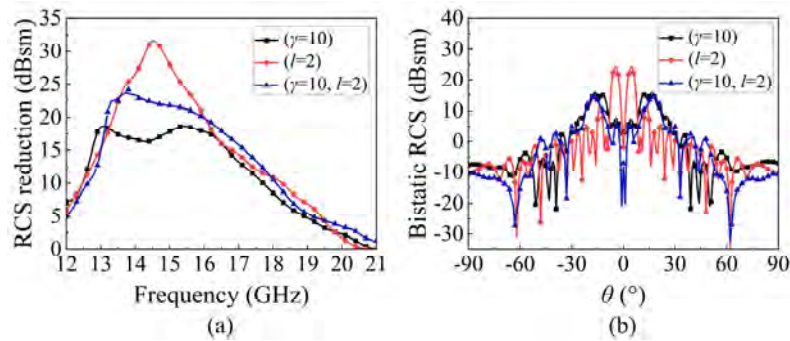


Fig. 8. Scattering performance comparison among different phase modulation strategies. (a) Monostatic RCS reduction curves compared to an equal-sized PEC plate. (b) 2D bistatic scattering patterns evaluated at 13.4 GHz.

components while maintaining low RCS in the specular direction. Due to wavefront distortion induced by cylindrical curvature, metasurfaces with high diffusion coefficients exhibit unique fan-shaped scattering patterns. This behavior indicates that the designed composite-phase metasurface preserves effective backward scattering suppression even under conformal deployment. The simulation results demonstrate the strong conformal adaptability of the proposed design and its capability to maintain favorable RCS reduction performance in curved configurations. It should be noted that while a 2.5 mm thick F4B substrate is relatively rigid material in practice, the conformal analysis presented here serves as an equivalent numerical study. Its primary purpose is to theoretically validate the electromagnetic robustness of the diffusion-vortex phase strategy against wavefront distortions caused by curved geometries. For practical conformal deployments, the proposed phase methodology can be readily implemented on thinner, flexible laminates without altering the underlying physical mechanisms.

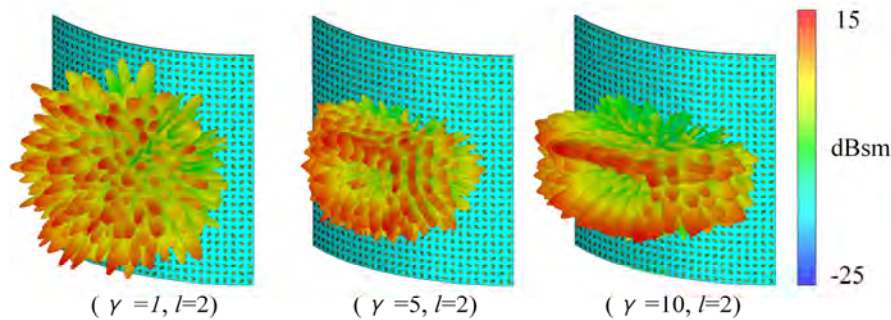


Fig. 9. 3D far-field scattering patterns of the cylindrically conformed metasurfaces at 15 GHz.

To evaluate the stealth performance of the conformal metasurface, a curved PEC plate with identical geometric parameters with curvature radius of 300 mm is introduced as a reference baseline. As shown in Fig. 10(a), the conformal metasurface achieves a substantial monostatic RCS reduction across the operating band compared to the curved PEC. Furthermore, Fig. 10(b) shows the bistatic scattering patterns reveal that the metasurface effectively reshapes the tangential scattering, significantly suppressing the strong reflections inherently caused by the curved metallic surface. This demonstrates that the proposed diffusion-vortex phase strategy maintains robust

scattering suppression even under severe curvature-induced wavefront distortions. This phase modulation methodology is highly adaptable and remains applicable when the design is transferred to thinner, flexible substrates for varying radii of curvature in future applications.

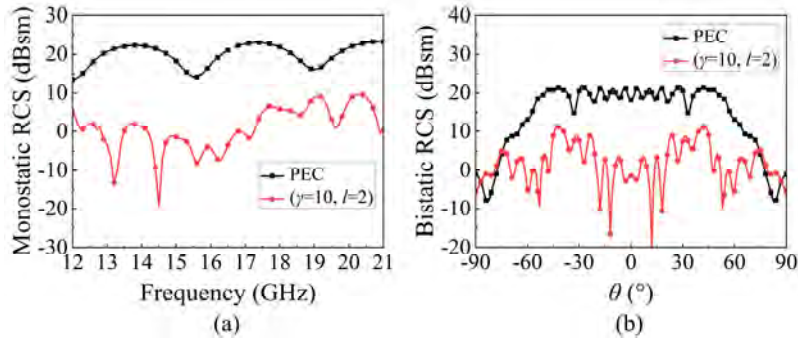


Fig. 10. Scattering performance between the conformal metasurface ($\gamma=10$, $l=2$) and a PEC cylinder of equivalent dimensions with a curvature radius of 300 mm. (a) monostatic RCS reduction and (b) bistatic scattering patterns at 15 GHz.

A quantitative performance comparison with existing RCS reduction metasurfaces is summarized in Table 1 to underscore the superiority of the proposed design. Prior works have successfully achieved significant broadband RCS reduction using coding and spatial phases [3], or polarization conversion mechanisms [9]. Furthermore, recent cutting-edge metasurfaces based on pure OAM mechanisms [22,26] have demonstrated remarkable capabilities, achieving extremely deep monostatic RCS reduction depths and broad bandwidths. However, for practical stealth applications, broadband monostatic reduction alone is not sufficient. Pure OAM mechanisms tend to redistribute the reflected energy into a concentrated annular bistatic scattering pattern. In contrast, the proposed diffusion-vortex metasurface introduces an additional diffusion phase to alleviate this issue by breaking the concentrated bistatic scattering ring into a broader and less localized angular distribution. For the representative design with ($\gamma=10$, $l=2$), it achieves a substantial maximum monostatic RCS reduction of 24.5 dB with a functional -10 dB bandwidth of 35.6%. While the design effectively suppresses both cross-polarized and co-polarized scattering, its most distinct advantage lies in its bistatic peak suppression capability. The synergistic dual-phase mechanism effectively breaks down the dangerous concentrated bistatic scattering ring inherent to pure vortex waves, diffusing it into uniform, low-level spatial background noise.

Table 1. Performance Comparison among Different RCS Reduction Metasurfaces

Ref.	Operating Mechanism	Bistatic peak suppression	-10 dB BW (%)	Max. RCS Reduction (dB)
[3]	Coding phase, Spatial phase	Yes	94.2%	20
[9]	Polarization conversion	No	103%	15
[22]	Pure OAM	No	6.5%	40
[26]	Vortex singularity	No	115.4%	53
This work	Diffusion-Vortex phase	Yes	35.6%	24.5

3. Experimental verification and discussion

Experimental validation of the proposed diffusion-vortex composite phase metasurfaces are conducted using 300 mm \times 300 mm fabricated samples with parameter combinations ($\gamma=1$, $l=2$)

and $(\gamma=10, l=2)$. Figure 11(a) shows the fabricated samples, while Fig. 11(b) presents the corresponding measurement environment. The RCS reduction performance is measured using a vector network analyzer connected to LCP transmitting horn and RCP receiving horn. In addition, the 2D co-polarized scattering patterns are measured using two LCP horn antennas.

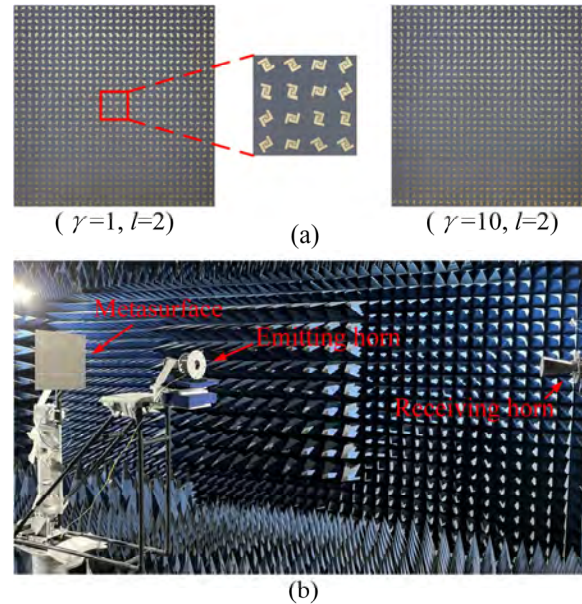


Fig. 11. Experiment validation of proposed metasurfaces, (a) fabricated samples and (b) measured environment.

Figure 12 presents the measured monostatic RCS reduction results of the metasurfaces with parameter combinations of $(\gamma=1, l=2)$ and $(\gamma=10, l=2)$. The measured results exhibit good agreement with the simulation results. For the metasurface with $(\gamma=1, l=2)$, an RCS reduction exceeding 10 dB is achieved over the frequency range from 12.35 GHz to 17.2 GHz, with a maximum measurement deviation of 1.69 dB. In contrast, the metasurface with $(\gamma=10, l=2)$ demonstrates more than 10 dB reduction across 12.63 GHz to 18.1 GHz and reaches a peak reduction of 20 dB reduction from 13.2 GHz to 15.94 GHz, corresponding to a relative bandwidth of 18.8% and a maximum deviation of 1.52 dB. These minor discrepancies originate from the inevitable fabrication tolerances and systematic measurement errors inherent to the experimental process.

Figure 13 presents the measured 2D E-plane far-field scattering patterns of the metasurface with $\gamma=1$ and $l=2$, which exhibits multiple uniformly diffused beams distributed over different directions within the frequency range from 13 GHz to 18 GHz. The experimentally observed beam diffusion angles show good agreement with the simulation results. Minor deviations in beam directions and power levels are observed, which can be attributed to antenna alignment inaccuracies during measurements and fabrication tolerances of the metasurface samples. Figure 14 shows the corresponding scattering patterns for the metasurface with $(\gamma=10, l=2)$, where a pronounced conical beam diffusion behavior is observed. In this case, electromagnetic reflections within the backward angular region of approximately 30° are significantly suppressed. The metasurfaces achieve effective RCS reduction within specified angular ranges, and the measured beam directions exhibit slight deviations from those of simulations at higher frequencies.

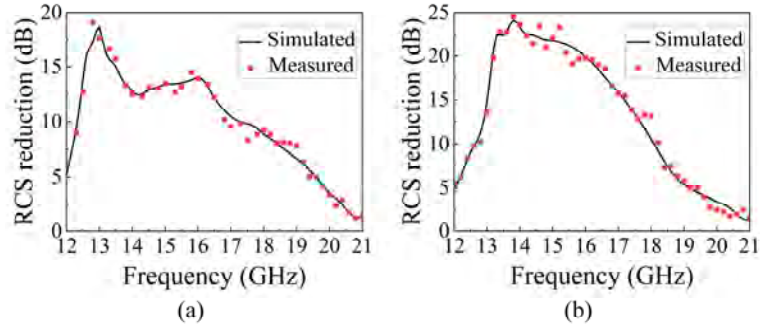


Fig. 12. Measured monostatic RCS reduction curve of the metasurface, (a) for $\gamma=1$ and $l=2$, and (b) for $\gamma=10$ and $l=2$.

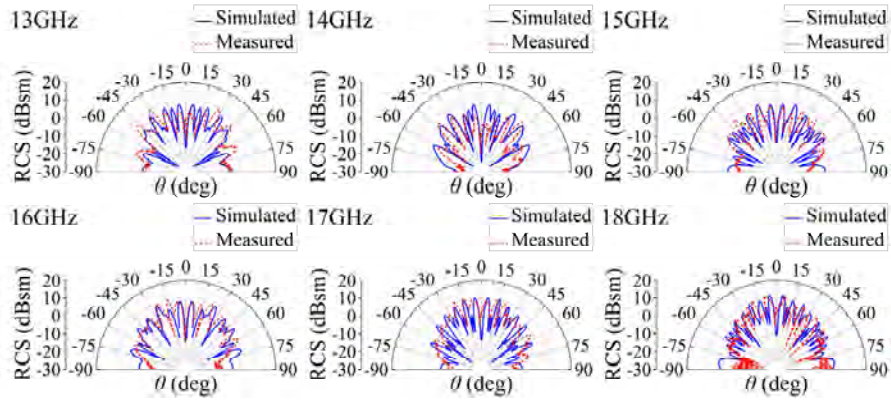


Fig. 13. Measured two-dimensional E-plane far-field scattering patterns of the metasurface with $\gamma=1$ and $l=2$.

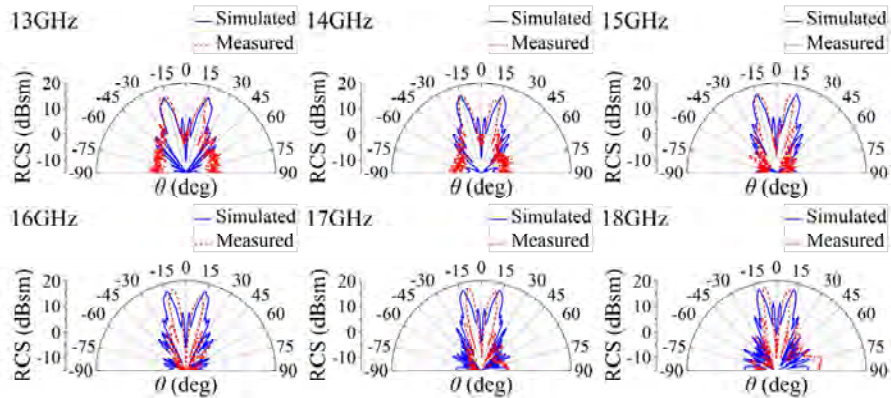


Fig. 14. Measured two-dimensional E-plane far-field scattering patterns of the metasurface with ($\gamma=10$, $l=2$).

4. Conclusions

This paper presents a diffusion-vortex composite phase metasurface. Under circularly polarized wave incidence, the metasurface converts the reflected energy into the co-polarized state, significantly reducing the cross-polarized component compared to a standard PEC target. Simultaneously, the co-polarized scattering beam is effectively diffused and suppressed by the composite phase modulation, achieving a distinct RCS reduction. The diffusive phase component generates uniformly diffused co-polarized scattering beam within a specific angular range, while the vortex phase component introduces a central null region. The scattering angles and null scope can be dynamic controlled by adjusting the diffusion coefficient γ and the vortex order l . The proposed approach remains effective when the metasurface is implemented in cylindrical conformal configurations. Simulation results demonstrate that the metasurface with $\gamma=1$ and $l=2$ achieves cross-polarized RCS reduction exceeding 10 dB over the frequency range from 12.35 GHz to 17.2 GHz (32.8%), corresponding to a relative bandwidth of 32.8%. For the metasurface with $\gamma=10$ and $l=2$, RCS reduction exceeding 10 dB and 20 dB is achieved over the frequency ranges from 12.63 GHz to 18.1 GHz (35.6%) and 13.2 GHz to 15.94 GHz (18.8%), respectively. Experimental measurements show good agreement with the simulation results in terms of both cross-polarized RCS reduction and co-polarized scattering characteristics. Furthermore, adding additional angle-dependent phase compensation terms can achieve RCS reduction for wide-angle or oblique incidence. The proposed metasurface effectively suppresses backward scattering of circularly polarized waves and provide a viable approach for metasurface-based stealth design.

Funding. National Natural Science Foundation of China (U2241204).

Disclosures. The authors declare that there are no conflicts of interest related to this article.

Data availability. Data underlying the results presented in this paper are not publicly available at this time but may be obtained from the authors upon reasonable request.

References

1. W. Chen, C. A. Balanis, and C. R. Birtcher, "Checkerboard EBG surfaces for wideband radar cross section reduction," *IEEE Trans. Antennas Propag.* **63**(6), 2636–2645 (2015).
2. M. K. T. Al-Nuaimi, W. Hong, and W. G. Whittow, "Aperiodic sunflower-like metasurface for diffusive scattering and RCS reduction," *IEEE Antennas Wireless Propag. Lett.* **19**(7), 1048–1052 (2020).
3. G. Y. Deng, Y. H. Zhang, H. T. Gao, *et al.*, "A super diffuse broadband RCS reduction surface design based on rotated phase coding polarization conversion metasurfaces," *IEEE Trans. Antennas Propag.* **71**(9), 7409–7417 (2023).
4. A. A. Khurram, N. Ali, S. A. Rakha, *et al.*, "Optimization of the carbon coating of honeycomb cores for broadband microwave absorption," *IEEE Trans. Antennas Propag.* **56**(5), 1061–1066 (2014).
5. C. H. Wang, H. X. Xu, Y. Z. Wang, *et al.*, "Hybrid-phase approach to achieve broadband monostatic/bistatic RCS reduction based on metasurfaces," *J. Phys. D: Appl. Phys.* **53**(36), 365001 (2020).
6. J. X. Su, Y. Y. Cui, Z. R. Li, *et al.*, "Metasurface base on uneven layered fractal elements for ultra-wideband RCS reduction," *AIP Adv.* **8**(3), 035027 (2018).
7. Z. H. Li, J. H. Wang, and W. Zheng, "Deformable transparent metasurface with multipolarization absorptive characteristics for RCS reduction," *IEEE Trans. Antennas Propag.* **73**(3), 1768–1776 (2025).
8. S. Ji, C. Jiang, J. Zhao, *et al.*, "An ultra-broadband metamaterial absorber with high absorption rate throughout the X-band," *Phys. Status Solidi (b)* **256**(11), 1900069 (2019).
9. Y. T. Jia, Y. Liu, Y. J. Guo, *et al.*, "Broadband polarization rotation reflective surfaces and their applications to RCS reduction," *IEEE Trans. Antennas Propag.* **64**(1), 179–188 (2016).
10. F. X. Li, H. Y. Chen, L. B. Zhang, *et al.*, "Compact high-efficiency broadband metamaterial polarizing reflector at microwave frequencies," *IEEE Trans. Microwave Theory Tech.* **67**(2), 606–614 (2019).
11. B. Q. Lin, W. Z. Huang, J. X. Guo, *et al.*, "Ultra-wideband radar cross-section reduction based on phase cancellation," *Electromagnetics* **43**(3), 151–162 (2023).
12. Q. Chang, J. Z. Ji, and Y. P. Ma, "Transparent and flexible chessboard metasurface based on optimized multielement phase cancellation for wideband RCS reduction," *IEEE Access* **12**, 27887–27894 (2024).
13. G. Z. Wu, W. Q. Yu, T. Lin, *et al.*, "Ultra-wideband RCS reduction based on non-planar coding diffusive metasurface," *Materials* **13**(21), 4773 (2020).
14. Q. Chang, J. Z. Ji, K. Chen, *et al.*, "Transparent and ultra-thin flexible checkerboard metasurface for radar-infrared bi-stealth," *Sensors* **24**(5), 1531 (2024).
15. X. Xie, M. B. Pu, J. J. Jin, *et al.*, "Generalized Pancharatnam-Berry phase in rotationally symmetric meta-atoms," *Phys. Rev. Lett.* **126**(18), 183902 (2021).

16. M. K. T. Al-Nuaimi, W. G. Whittow, G. L. Huang, *et al.*, "Wideband radar-cross-section reduction using parabolic phased metasurfaces," *IEEE Antennas Wireless Propag. Lett.* **22**(7), 1547–1551 (2023).
17. H. X. Xu, G. M. Wang, T. Cai, *et al.*, "Tunable Pancharatnam–Berry metasurface for dynamical and high-efficiency anomalous reflection," *Opt. Exp.* **24**(24), 27836–27848 (2016).
18. W. M. Pan and J. S. Li, "Diversified functions for a terahertz metasurface with a simple structure," *Opt. Exp.* **29**(9), 12918–12929 (2021).
19. Z. X. Zhu and X. Zhou, "Study on electromagnetic focusing with fully phase-adjustable high transmittance metasurface," *Electronics* **14**(4), 669 (2025).
20. Y. Y. Yuan, S. Q. Chen, B. Ratni, *et al.*, "Bi-functional meta-device with full energy utilization in co- and cross-polarization fields," *Appl. Phys. Lett.* **117**(17), 171602 (2020).
21. T. Liu, X. M. Fu, J. F. Wang, *et al.*, "Single-layer achiral metasurface with independent amplitude–phase control for both left-handed and right-handed circular polarizations," *ACS Appl. Mater. Interface* **14**(29), 33968–33975 (2022).
22. Q. Liu, H. Y. Chen, Y. Y. Yan, *et al.*, "RCS reduction metasurface based on orbital angular momentum," *Results Phys.* **53**, 107008 (2023).
23. S. Wu, Y. H. Zhang, X. D. Cui, *et al.*, "Generation of dual-polarization orbital angular momentum vortex beams with reflection-type metasurface," *Optics Commun.* **553**, 130107 (2024).
24. J. Wang, J. Y. Yang, I. M. Fazal, *et al.*, "Terabit free-space data transmission employing orbital angular momentum multiplexing," *Nat. Photonics* **6**(7), 488–496 (2012).
25. W. Geng, Q. X. Guo, J. X. Su, *et al.*, "Dartboard Metasurface for RCS Reduction and OAM Wave Generation," *IEEE Trans. Antennas Propag.* **73**(4), 2497–2509 (2025).
26. Q. Liu, D. F. Liang, X. Yao, *et al.*, "Broadband RCS reduction metasurface based on vortex singularities generated by Spin-to-Orbital angular momentum conversion," *Results Phys.* **59**, 107530 (2024).
27. J. Y. Ren, M. Z. Hu, X. Y. Pang, *et al.*, "OAM-focal shift coupling effect and its application in wideband and angularly stable RCS reduction," *Photonics Res.* **14**(1), 241–255 (2026).
28. C. H. Xue, H. C. Zhao, T. Li, *et al.*, "Efficient generation of a dual-polarized vortex wave with an ultrathin Huygens' metasurface," *Opt. Exp.* **30**(21), 39175–39187 (2022).
29. X. N. Hui, S. L. Zheng, Y. P. Hu, *et al.*, "Ultralow reflectivity spiral phase plate for generation of millimeter-wave OAM beam," *IEEE Antennas Wireless Propag. Lett.* **14**, 966–969 (2015).
30. S. M. Mohammadi, L. K. S. Daldorff, J. E. S. Bergman, *et al.*, "Orbital angular momentum in radio—a system study," *IEEE Trans. Antennas Propag.* **58**(2), 565–572 (2010).
31. H. X. Xu, H. W. Liu, X. H. Ling, *et al.*, "Broadband vortex beam generation using multimode Pancharatnam–Berry metasurface," *IEEE Trans. Antennas Propag.* **65**(12), 7378–7382 (2017).
32. G. W. Ding, K. Chen, X. Y. Luo, *et al.*, "Dual-Helicity decoupled coding metasurface for independent spin-to-orbital angular momentum conversion," *Phys. Rev. Applied* **11**(4), 044043 (2019).
33. L. J. Yang, S. Sun, and W. E. I. Sha, "Ultra-wideband reflection-type metasurface for generating integer and fractional orbital angular momentum," *IEEE Trans. Antennas Propag.* **68**(3), 2166–2175 (2020).
34. N. Yu, P. Genevet, M. A. Kats, *et al.*, "Light propagation with phase discontinuities: generalized laws of reflection and refraction," *Science* **334**(6054), 333–337 (2011).